Journal of The Electrochemical Society, **153** (3) G197-G202 (2006)
0013-4651/2006/153(3)/G197/6/$20.00 © The Electrochemical Society

Investigation of Molybdenum Nitride Gate on SiO_2 and HfO_2 for MOSFET Application

Bing-Yue Tsui,[a,b,z] Chih-Feng Huang,[a] and Chih-Hsun Lu[a]

[a]*Department of Electronics Engineering and Institute of Electronics, National Chiao Tung University, Hsinchu 300, Taiwan*
[b]*National Nano Device Laboratories, Hsinchu 300, Taiwan*

It has been reported that the work function of nitrided molybdenum (MoN) can be modulated by the atomic ratio of N/Mo and is suitable for gate material of complementary metal oxide semiconductor devices. In this work, we investigated the characteristics of MoN_x prepared by reactively sputtering deposition from the gate electrode point of view. The main phase of the MoN_x films is MoN(200). As the N/Mo ratio increases, the microstructure of MoN_x film tends to be amorphous-like and the resistivity increases. After high-temperature annealing, the phase remains stable and grain size increases slightly. The HfO_2 film has better immunity to sputtering damage than SiO_2 film; therefore, the sputtering deposition method could be a choice of metal gate deposition as HfO_2-based dielectric is used. The work function of MoN_x increases with the increase of nitrogen content and tends to saturate at the valence band of Si. No Fermi-pinning effect is observed on HfO_2 film. The work function and thermal stability of MoN_x show good thermal stability on both SiO_2 and HfO_2 films up to 800°C at least. All of these results indicate that MoN is a good candidate of gate electrode for p-type metal oxide semiconductor field effect transistors (pMOSFETs) or fully depleted SOI devices.
 [DOI: 10.1149/1.2158576]

Manuscript submitted April 13, 2005; revised manuscript received September 27, 2005. Available electronically January 23, 2006.

Metal gates are expected to replace polysilicon gates beyond the 45-nm technology node, according to the ITRS roadmap.[1] Suitable work function (Φ_m) and chemical inertia of metal gates are the two main criteria for proper threshold voltage and easy device integration, respectively. The work function of metal gates should be 4.1–4.4 eV for bulk n-type metal oxide semiconductor field effect transistors (nMOSFETs) and 4.8–5.1 eV for bulk p-type MOSFETs (pMOSFETs).[2,3] The chemical inert metal gates should be thermally stable enough to avoid chemical reaction with gate dielectric and the surrounding insulators during source/drain dopant activation. With these properties, metal gates could be suitable for the conventional gate process, which is much simpler than the replacement gate process.[4-10] Actually, for the complementary metal oxide semiconductor (CMOS) fabricated with conventional gate process, dual-work-function metal gates would still be crucial if two different metal gate materials are required.[11,12] The significant challenges are removing the gate materials without damaging the underlying dielectric and simultaneous patterning different gate electrodes.

Molybdenum (Mo) films have drawn a lot of attention as a single metal gate electrode of CMOS devices because the work function of Mo on SiO_2 can be adjusted from 4.36 to 4.95 eV.[13-18] Moreover, molybdenum has low resistivity, good thermal stability, and high density, which is a benefit for ion-implantation mask.[15,16] The work function of molybdenum varies with the bulk microstructure, which depends on the deposition and annealing conditions.[17,18] It can also be modulated by the implantation of nitrogen or argon.[2,18-21] The work function of the (110)-oriented Mo film is 4.95 eV. After nitrogen implantation to produce Mo_2N phase, the work function can be lowered.[18,21] However, the work function of Mo film on high-k dielectric, such as $ZrSiO_4$ or Si_3N_4, is quite different from that on SiO_2 and it is also thermally unstable.[14,21] This observation was explained by the Fermi pinning effect due to interfacial dipole formation or minimum interfacial reaction.[22-26]

In this work, we first discuss the thermal stability of MoN_x film deposited by reactive sputtering with different nitrogen atomic ratios and then examine the work function variations, as well as the Fermi pinning phenomenon, on SiO_2 and HfO_2 after annealing at different temperatures. Moreover, the sputtering damage, during MoN_x deposition, was also investigated.

[z] E-mail: bytsui@mail.nctu.edu.tw

Experimental

Sample preparation.— Simple metal oxide semiconductor (MOS) capacitors were used as the test devices. The starting material was 6-in., (100)-oriented, and boron-doped p-type silicon wafers with a resistivity of 15–25 Ω cm. Oxide layers with various thicknesses of 40, 70, or 100 nm was thermally grown in dry O_2 ambient. Some wafers were deposited by a 5-nm-thick HfO_2 layer in a reactively sputtered deposition system with an Ar/O_2 gas-flow ratio of 24:3 sccm. During deposition, the chamber pressure was at 7.6 mTorr, the dc sputtering power was 100 W, and neither substrate bias nor heating was intentionally applied. Because the bottom oxide is thick enough, additional oxidation during HfO_2 deposition will not occur. After the preparation of gate dielectrics including SiO_2 single layer and HfO_2/SiO_2 stack, all wafers were annealed at 900°C in N_2 ambient for 30 s in a rapid thermal annealing (RTA) system in order to reduce the oxide charges and make the microstructure of HfO_2 stable during the postmetal anneal. A lift-off process was used to define the metal gate electrode. The MoN_x films with various Mo/N atomic ratios were reactively sputtered at 4.5 mTorr in a dc sputtering system to a thickness of 60 nm, with Ar/N_2 gas-flow ratios of 20:0, 20:5, 20:10, and 20:20. During deposition, the dc sputtering power was set to 25 W and neither substrate bias nor substrate heating was intentionally applied. Some wafers were deposited at 50 or 100 W to investigate the sputtering damage. After the lift-off process, wafers were cut into small pieces and were rapid thermal annealed at 400, 500, 600, 700, and 800°C for 30 s in N_2 ambient. The gate electrode is circular shape with diameter of 400 μm. Finally, the aluminum film was deposited on the wafer back side by thermal evaporation to establish good ohmic contact.

The atomic composition of MoN_x samples were identified by Rutherford backscattering spectroscopy (RBS). A graphite substrate was used instead of the silicon substrate to avoid the weak nitrogen signal from the MoN_x layer being overlapped with the strong Si signal from the substrate. A 30-nm-thick SiO_2 layer was deposited in a plasma-enhanced chemical vapor deposition (PECVD) system on graphite substrate before MoN film deposition to provide a similar surface condition with real SiO_2/Si samples. The crystalline phase of the MoN_x films was examined by the X-ray diffraction (XRD) technique. The sheet resistance of the MoN_x films was measured by four-point-probe method.

The capacitance-voltage (C-V) curves of the capacitors were measured at 100 kHz by a precision impedance meter of model Agilent 4284A, and then flatband voltage (V_{FB}) was extracted from the C-V curves. The current-voltage (I-V) curves were measured by

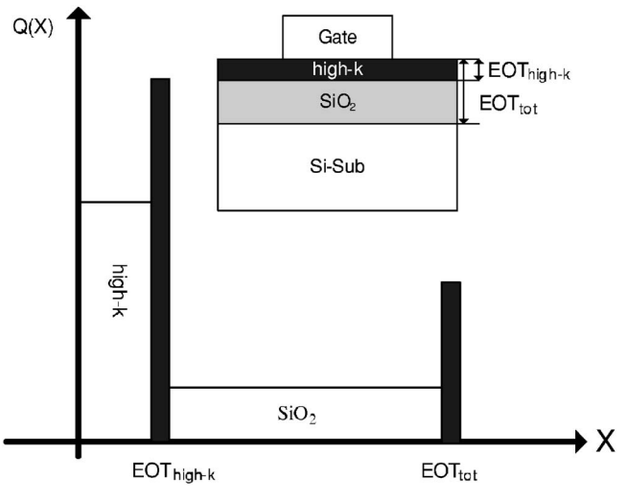

Figure 1. Schematic plot of charge distribution in the $HfO_2/SiO_2/Si$ structure. The bulk charge in SiO_2 and HfO_2 films is assumed to be a uniform distribution.

a semiconductor parameter analyzer of model Agilent 4156C. The method of work function extraction is explained in the next subsection.

Work function extraction.— The widely used method to extract work function of metal gates on oxide is extrapolating the flatband voltage (V_{FB}) to zero equivalent oxide thickness (EOT) from the V_{FB} vs EOT plot. The V_{FB} is defined as

$$V_{FB} = \Phi_m - \Phi_{Si} - \frac{Q_{eff}}{\varepsilon_{ox}} EOT \quad [1]$$

where Φ_m and Φ_{Si} are the work function of metal gate and silicon, respectively, Q_{eff} is the equivalent oxide charges per unit area, and ε_{ox} is the dielectric constant of SiO_2.[27] The Q_{eff} reflects the total effect of the interface trap charges (Q_{it}), the fixed oxide charges (Q_f), the oxide charges (Q_{ox}), and the mobile charges (Q_m). Actually, V_{FB} should be expressed as

$$V_{FB} = \Phi_m - \Phi_{Si} - \frac{1}{\varepsilon_{ox}}\left[\int_0^{EOT} x\rho(x)dx\right] \quad [2]$$

where $\rho(x)$ is the charge distribution in gate dielectric. Therefore, as the bulk charge density is not low enough, Eq. 1 cannot be applied to extract Φ_m because of the nonlinear behavior of the V_{FB}-*EOT* relationship. For many high-*k* dielectrics, such as HfO_2 used in this work, the bulk charge is not negligible.[28] This would result in failure of the conventional work function extraction method by changing high-*k* dielectric thickness.

In this work, we propose a simple method of using high-*k*/SiO_2 stack with constant high-*k* dielectric thickness and different SiO_2 thickness according to Ref. 28. The bottom SiO_2 layer can avoid the formation of interfacial layer between high-*k* dielectric and Si substrate. With constant high-*k* dielectric thickness, the charges related to high-*k* dielectric, bulk charge in high-*k* dielectric, and interface charge at high-*k* dielectric/SiO_2 charge are fixed. The charge distribution of the stack structure is shown in Fig. 1 schematically. The V_{FB} derived from Eq. 2 is expressed as

$$V_{FB} = \Phi_m - \Phi_{Si} - \frac{1}{\varepsilon_{ox}}\left[\frac{1}{2}\rho_{high\text{-}k}EOT_{high\text{-}k}^2 + Q_{high\text{-}k}EOT_{high\text{-}k} - \frac{1}{2}\rho_{SiO_2}EOT_{high\text{-}k}^2\right] - \frac{1}{\varepsilon_{ox}}[Q_{SiO_2}EOT_{tot}] - \frac{1}{\varepsilon_{ox}}\left[\frac{1}{2}\rho_{SiO_2}EOT_{tot}^2\right] \quad [3]$$

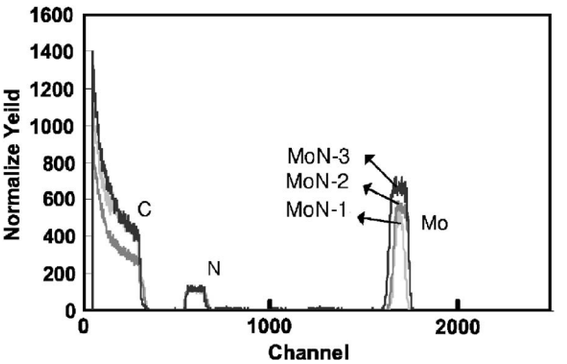

Figure 2. RBS spectra of MoN_x films on graphite substrate.

The $\rho_{high\text{-}k}$ and ρ_{SiO_2} are the uniform bulk charge density of high-*k* dielectric and SiO_2 layer, respectively. It is noted is not necessary that these two charges be uniformly distributed. In that case integral form should be used in Eq. 3. The $Q_{high\text{-}k}$ and Q_{SiO_2} are the interface charges at the high-*k* dielectric/SiO_2 interface and the SiO_2/Si interface, respectively. The $EOT_{high\text{-}k}$ and EOT_{tot} are the effective oxide thickness of the high-*k* dielectric layer only and the effective oxide thickness of the whole high-*k* dielectric/SiO_2 stack.[28] With fixed high-*k* layer thickness, the flatband voltage is a linear function of EOT_{tot}, because the first bracket term is constant $\left(Q_o = \frac{1}{2}\rho_{high\text{-}k}EOT_{high\text{-}k}^2 + Q_{high\text{-}k}EOT_{high\text{-}k}\right)$ and the last term can be eliminated on account of the small bulk oxide charge in SiO_2 layer. At first, we assume that the last term of Eq. 3 is negligible as $\rho_{SiO_2}EOT_{tot} < Q_{SiO_2}$. The validity of this assumption has been approved.[28] The bracket of the 3rd term is independent of EOT_{tot} and is represented by Q_o. In this case, Eq. 3 can be simplified to be

$$V_{FB} = \Phi_m - \Phi_{Si} - \frac{Q_o}{\varepsilon_{ox}} - \frac{1}{\varepsilon_{ox}}[Q_{SiO_2}EOT_{tot}] \quad [4]$$

The flatband voltage extracted by this method is the work function of metal on high-*k* dielectric with an offset value accounting for the charges of the high-*k* layer. As the $EOT_{high\text{-}k}$ is low enough, the two $EOT_{high\text{-}k}^2$ terms in the first bracket of Eq. 3 become negligible. Hence, the Q_o accounts for the interface charge at high-*k*/SiO_2 interface.

The purpose of using thick bottom SiO_2 in this work is to simplify the extraction of work function difference. The work function difference is extrapolated from the V_{FB}-*EOT* plot. However, only the capacitance equivalent thickness (CET) can be measured directly. Quantum effect correction must be used to transform CET to EOT if gate dielectric is thin. Because the work function difference is independent of EOT, it is not necessary to use a thin SiO_2 layer. Using a thick-bottom SiO_2 can neglect quantum correction and simplify the data processing.

Results and Discussion

Physical properties of MoN_x films.— Figure 2 shows the RBS spectrum of MoN_x films deposited on graphite substrate with various Ar/N_2 gas-flow ratios of 20:5, 20:10, and 20:20. Due to the use of graphite substrate instead of Si substrate, the nitrogen signals can be resolved clearly and the N/Mo atomic ratio can be determined precisely. The respective N/Mo atomic ratios are 0.85, 1, and 1.45.

Figure 3 shows the XRD spectra of MoN_x films annealed at different temperatures in N_2 ambient for 30 s. Strong MoN(200) phase was detected over all samples. With the increase of annealing temperature, the intensity of MoN(200) phase increases. The increasing intensity of MoN(200) signal implies grain growth during high-temperature annealing. Looking into the XRD spectra, the higher the nitrogen content is, the weaker the MoN(200) signal in-

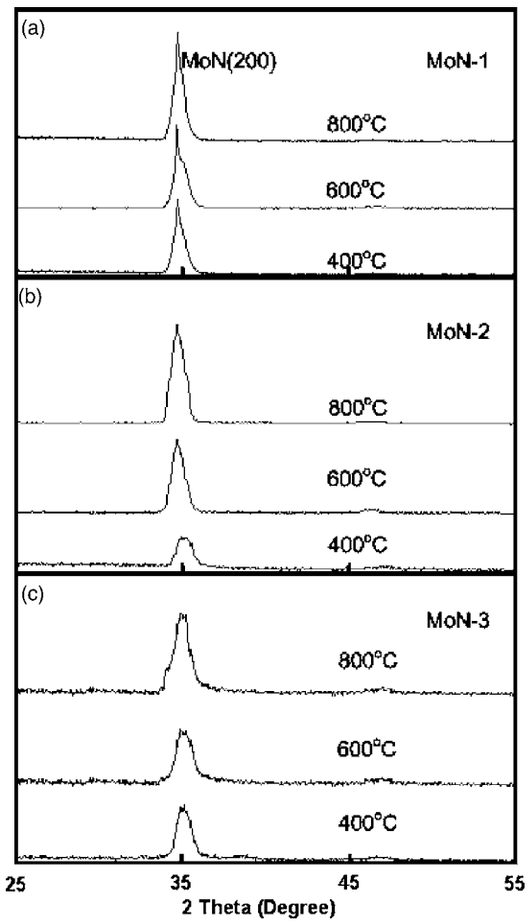

Figure 3. XRD spectra of (a) MoN-1, (b) MoN-2, and (c) MoN-3 films after annealing at different temperatures.

tensity is. This phenomenon implies that the excess nitrogen can make the MoN_x films tend to be amorphous-like. However, the drawback of high nitrogen content in the MoN_x is the high resistivity of the film. As the annealing temperature increases, the sheet resistance decreases due to grain growth but the higher nitrogen content samples still show higher resistivity. Table I lists the MoN_x films' ID and summarizes the above material characteristics.

When the atomic ratio of N/Mo is less than 0.40, the main phase is Mo. With the increase of nitrogen content ranging from 0.40 of atomic ratio to 0.54, the main phase is Mo_2N including β-Mo_2N and γ-Mo_2N. The β-Mo_2N will transfer into the γ-Mo_2N phase at higher temperature anneal and higher nitrogen content. The nitrogen content ranged from 0.54 to 0.67; the main phase is Mo_3N_2. Furthermore, molybdenum nitride with nitrogen content higher than 0.67 has the main phase of MoN.[29] In this work, the N/Mo atomic ratio is higher than 0.85 so that molybdenum nitride has the main phase of MoN.

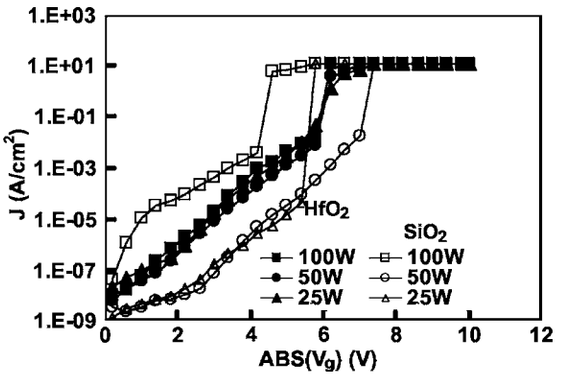

Figure 4. C-V characteristic of MoN/SiO_2(5 nm)/Si and MoN/HfO_2(5 nm)/Si capacitors with MoN film deposited at different powers. The current is measured at negative gate bias.

Sputtering damage.— During sputtering deposition, physical bombardment of metal atoms may damage gate dielectric.[30] To evaluate the sputtering damage of MoN_x film deposition, MoN-2 film of 60 nm was deposited on SiO_2(5 nm)/Si and HfO_2(5 nm)/Si substrates at various sputtering powers. The 5-nm-thick HfO_2 film was deposited on a HF-dipped Si substrate. The postdeposition annealing was performed at 900°C in N_2 ambient for 30 s in a RTA system. The postmetallization annealing was performed at 400°C in N_2 ambient for 30 s in the same RTA system. Figure 4 shows the typical I_g-V_g characteristics of all samples measured in accumulation mode. With the increase of sputtering power from 25 to 100 W, the leakage current of the SiO_2 samples increases. In contrast, the leakage current of HfO_2 samples is not affected by the sputtering power, although the leakage current of the HfO_2 samples is higher than that of the SiO_2 samples deposited at 25 and 50 Watts due to narrower bandgap and thinner EOT of the HfO_2 films. Therefore, it is presumed that the bombardment damage can be scaled with the sputtering power, and the HfO_2 layer has better immunity to bombardment damage due to high density and heavy Hf atoms. This presumption is verified by measuring the penetration of Mo atoms into dielectric.

After the removal of MoN gates by H_2SO_4/H_2O_2 mixture, the surface layer of gate dielectric was etched by dilute HF solution (DHF) and HF/isopropyl alcohol (IPA) mixture for SiO_2 and HfO_2, respectively. The Mo content in solutions was analyzed by the inductively coupled plasma mass spectrometry (ICP-MS). The Mo content in SiO_2 is shown in Fig. 5a. It is clear that Mo penetrates into the SiO_2 layer at least 2 nm. Moreover, the concentration of the Mo depends on the sputtering power. Figure 5b shows the Mo content in the HfO_2 layer. Up to 100 W sputtering power, Mo in the HfO_2 layer is still under the detecting limit of Mo by ICP-MS, which is about 0.2 ppb, i.e., 3×10^{17} atoms/cm^3. This result confirms that the heavy and dense HfO_2 film is more immune to bombardment damage than SiO_2 film. Sputtering deposition may be not a suitable method for metal gate deposition on SiO_2 dielectric but could be a choice for some high-*k* dielectric films. In the following

Table I. Sample ID and some basic characteristics.

ID	MoN-0	MoN-1	MoN-2	MoN-3
N/Mo atomic ratio	0	0.85	1	1.45
Phase	(110), (200), (211), (220)	MoN (200)	MoN (200)	MoN (200)
Resistivity (μΩ cm) (as-deposited)	178	650	1158	1736
Resistivity (μΩ cm) (after 600°C annealing)	86.7	464	832	1135

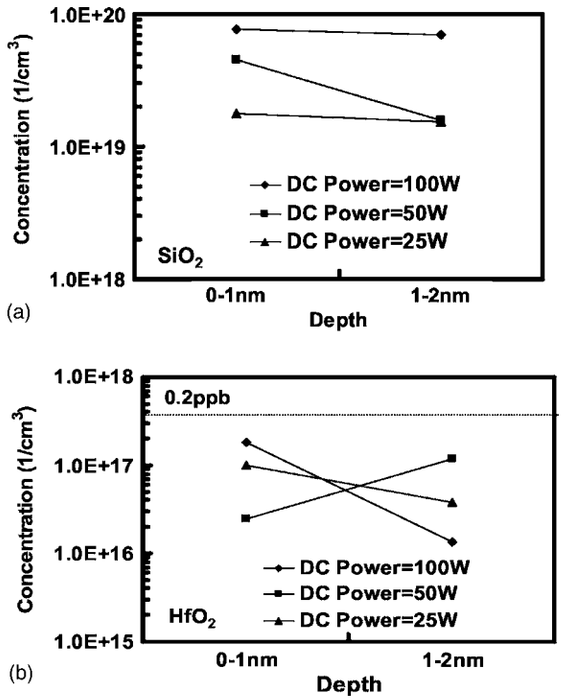

Figure 5. Mo concentration in (a) SiO_2 film of the MoN/SiO_2 structures and (b) HfO_2 film of the MoN/HfO_2 structure detected by ICP-MS.

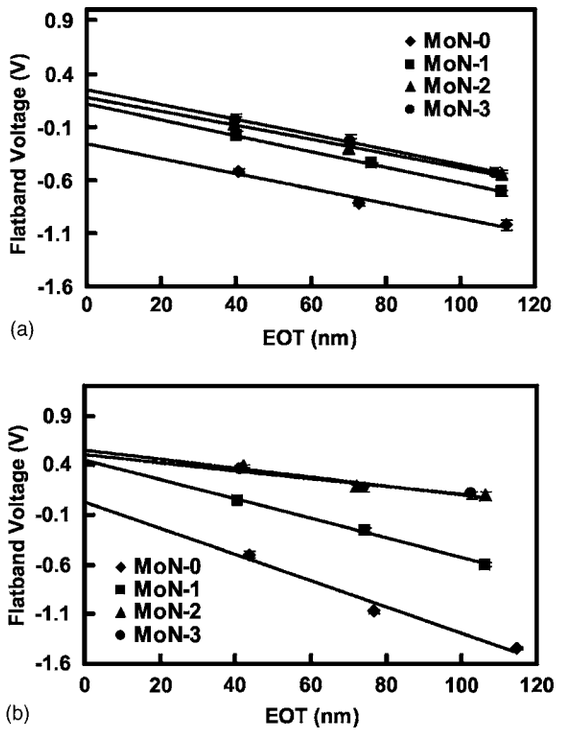

Figure 6. V_{FB} vs EOT plot of (a) $MoN_x/SiO_2/Si$ structure and (b) $MoN_x/HfO_2/SiO_2/Si$ structure after annealing at 500°C.

subsections, the sputtering power was set at 25 W for both the SiO_2 and HfO_2 sample. The sputtering rate of MoN at 25 W is about 2 nm/min.

Work function on SiO_2 and HfO_2.— Figure 6a and b shows the flatband voltage (V_{FB}) vs EOT plot of the 500°C-annealed samples with SiO_2 and HfO_2/SiO_2 stack as gate dielectric, respectively, where the V_{FB} values are the average from more than ten samples. The good linearity reflects the validity of Eq. 1 and 4. According to Eq. 1, the y axis interception in the V_{FB}-EOT plot represents the work function difference between metal gates and Si substrate ($\Phi_{ms} = \Phi_m - \Phi_{Si}$). While according to Eq. 4, the y axis interception in the V_{FB}-EOT plot represents the work function difference (Φ_{ms}) plus the effect of the HfO_2/SiO_2 interface charges ($Q_{high\text{-}k}$). With known Si substrate concentration, the work function of metal gate on SiO_2 layer can be extracted. However, on the HfO_2 layer, an offset due to the $Q_{high\text{-}k}$ are inevitable. We denote the offset value as Φ'_m.

The Φ_m of MoN_x films on SiO_2 and Φ'_m of MoN_x films on HfO_2 extracted from the V_{FB}-EOT plots are shown in Fig. 7a and b, respectively. The Φ_m and Φ'_m of MoN_x films are almost independent of the annealing temperatures but are dependent on the nitrogen content. This is one of the advantages of MoN_x because the work function of several metals changes after thermal annealing.[31] The MoN_x films on SiO_2 with N/Mo atomic ratios of 0, 0.85, 1, and 1.45 have work functions of 4.60, 4.97, 5.03, and 5.11 eV, respectively, after 500°C annealing. Compared with the MoN-0 sample, the increase of work function ($\Delta\Phi_m$) is 0.37, 0.43, and 0.51 eV as the N/Mo ratio is 0.85, 1, and 1.45, respectively. The increase of work function is not linearly dependent on the nitrogen composition. It increases rapidly with the addition of nitrogen and then gradually saturates at high nitrogen concentration. It is concluded that the work function of MoN_x film on SiO_2 can be adjusted by nitrogen incorporation from midgap to close to valance band of Si and can be applied as a gate electrode of bulk pMOSFETs or fully depleted silicon on insulator pMOSFETs.

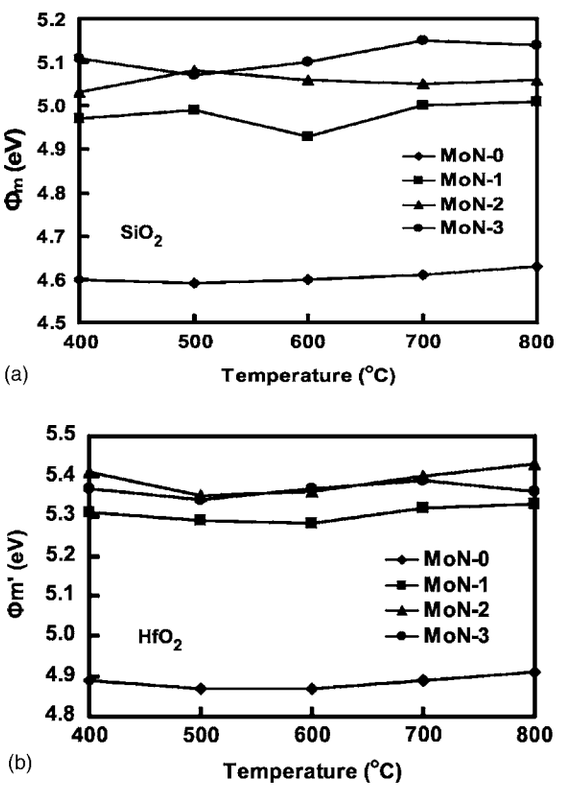

Figure 7. (a) Work function of MoN_x film on SiO_2 layer and (b) quasi-work function of MoN_x film on HfO_2 layer vs annealing temperature.

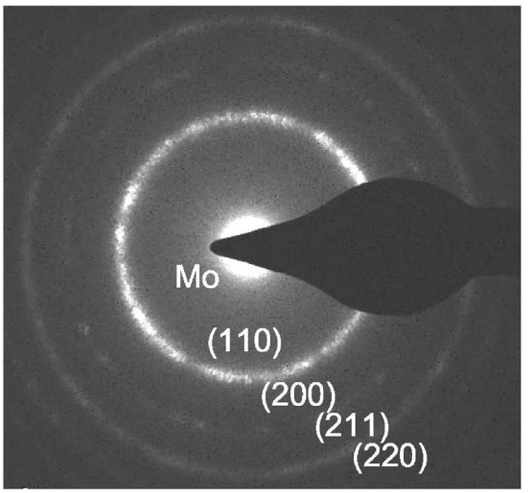

Figure 8. The electron diffraction pattern of the MoN-0 film after annealing at 600°C.

The Φ'_m values of MoN_x films on HfO_2 layers with N/Mo atomic ratios of 0, 0.85, 1, and 1.45 are 4.89, 5.31, 5.41, and 5.37 eV, respectively, after 500°C annealing. Because the HfO_2/SiO_2 stacks were prepared simultaneously and HfO_2 film is immune to sputtering damage, as discussed in a previous subsection, it is reasonable to assume that the $Q_{high\text{-}k}$ values are independent of gate electrode. The increase of work function, excluding the effect of $Q_{high\text{-}k}$, is 0.42, 0.52, and 0.48 eV as the N/Mo ratio is 0.85, 1, and 1.45, respectively. It is important that the magnitude of work function adjustment ($\Delta\Phi_m$) on HfO_2 film is nearly the same as that on SiO_2 film.

The Φ_m and Φ'_m of samples with the same MoN_x film and annealing conditions has a difference of about 0.3 eV over all samples. It is necessary to determine whether the interface dipole layer at the MoN_x/HfO_2 interface induces the Fermi pinning effect. The formation of interface dipole is due to the interaction of gate material and gate dielectric. The pinned Fermi energy should depend on gate material. Furthermore, the reported Fermi pinning effect always forces the work function of metal gates to the midgap of silicon. Both phenomena are not observed in this work. The Φ'_m of MoN_x films on HfO_2 shifts toward the valence band of silicon. Moreover, compared with MoN-0 film, the work function increase of MoN_x films incorporated with the same nitrogen on both SiO_2 and HfO_2 is almost the same. Therefore, it is believed that Fermi pinning does not occur in the MoN_x/HfO_2 stack. This is an important advantage for MoN films as gate electrode because it is quite possible that metal gate integrates with high-*k* dielectric while Hf-based dielectrics are promising. The 0.3-eV shift between Φ_m and Φ'_m is attributed to $Q_{high\text{-}k}$ now. After a simple calculation, the $Q_{high\text{-}k}$ is -1×10^{13} cm^{-2}, which is consistent with that reported in literature.[28]

The extracted work function of pure Mo film (MoN-0) on SiO_2 is 4.6 eV in this work. This value is different from the results of some literature. The work function of Mo depends on its crystalline orientation. There are several possible orientations of Mo film deposited by sputtering. Among them, only the (110) orientation has a work function close to the valence band of Si. The other orientations show work functions close to the midgap of Si.[17] Figure 8 shows the electron diffraction pattern of the 600°C-annealed Mo film. Although (110) is the dominant orientation, several crystalline orientations including (200), (211), and (220) are also identified. Therefore, the work function of the MoN-0 sample of 4.6 eV is reasonable and is consistent with other works,[15-17] although some recent papers reported that the work function is reduced by implanting nitrogen into Mo(110) film. The nitrogen concentrations are not high enough so that the main phase is Mo_2N in those works.[2,18-21] In this work,

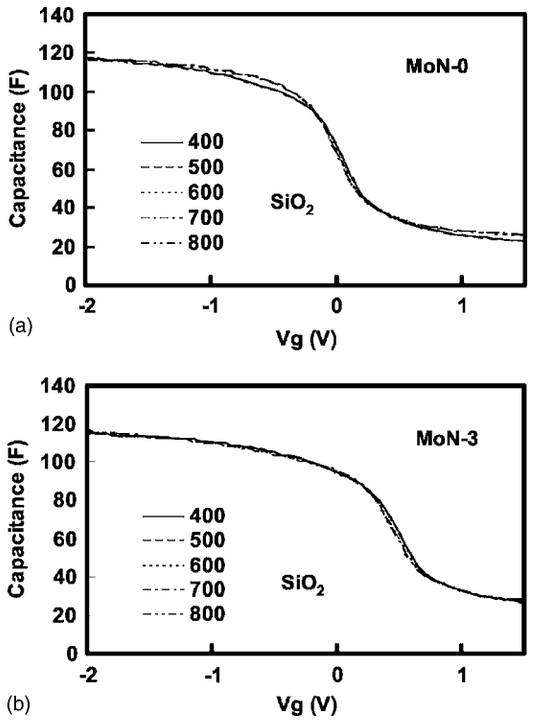

Figure 9. C-V curves of MoN_x(60 nm)/SiO_2(40 nm)/Si structure of (a) MoN-0 and (b) MoN-3 films after annealing at different temperatures.

Mo-nitride films were prepared by reactive sputtering technique and the N/Mo ratio is around unity. As shown in Fig. 3, the main phase of our samples is MoN(200) but not Mo_2N. Therefore, the different observation between our work and the references could be explained as follows. As the orientation of Mo film is pure (110), the work function is close to the valance band of Si. Nitrogen implantation destroys the (110) crystalline and the Mo film becomes amorphous. After annealing, the phase is Mo_2N due to insufficient nitrogen concentration. The work function of Mo_2N is close to the midgap of Si. Therefore, the higher the nitrogen implantation dose, the lower the work function is. Once the nitrogen concentration is high enough and the phase changes to be MoN, the work function increases. The work function of MoN is close to the valence band of Si, while the work function of Mo_2N is close to the midgap of Si.

Thermal stability.— Figure 9a and b shows the C-V curves of MoN-0 and MoN-3 samples, respectively, after annealing at different temperatures. The gate dielectric is a 40-nm-thick SiO_2 film. Slight distortion of the C-V curves at weak accumulation mode is observed for the MoN-0 sample annealed at temperatures below 600°C, and the distortion can be recovered after annealing at higher temperature. The distortion should be attributed to the interface states between gate dielectric and Si substrate.

Similarly, the C-V curves of HfO_2 samples with HfO_2(5 nm)/SiO_2(40 nm) stack gate dielectric are shown in Fig. 10. No distortion of C-V curves is observed. This observation confirms that HfO_2 is more immune to sputtering damage than SiO_2 previously. The accumulation capacitance of all SiO_2 and HfO_2 samples is almost the same. This result confirms the thermodynamic stability of HfO_2/thick SiO_2 stack.[31] All these results indicate that MoN_x films on both SiO_2 and HfO_2 layers are thermally stable up to 800°C. This result is better than several metals such as TiN, TaN, and TaSiN.[32]

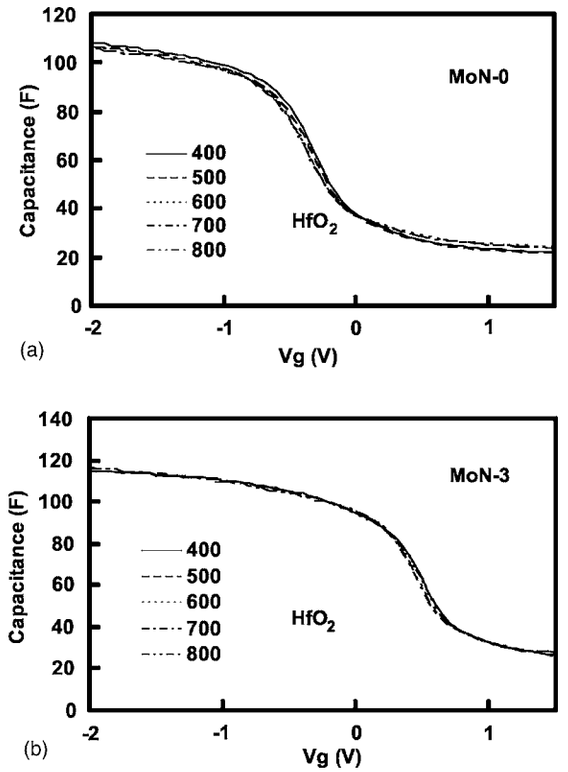

Figure 10. C-V curves of MoN_x(60 nm)/HfO_2(5 nm)/SiO_2(40 nm)/Si structure of (a) MoN-0 and (b) MoN-3 films after annealing at different temperatures.

Conclusions

We investigated the work function modulation and thermal stability of MoN_x films with different nitrogen contents. The N/Mo atomic ratios of MoN_x films analyzed by the RBS are 0.85, 1.0, and 1.45. Several important observations are summarized as follows:

1. The main phase of the MoN_x films is MoN(200). As the N/Mo ratio increases, the microstructure of MoN_x film tends to be amorphous-like and the resistivity increases. After high-temperature annealing, the phase remains stable and grain size increases slightly.

2. The HfO_2 films have better immunity to sputtering damage; therefore, sputtering deposition could be a choice of metal gate deposition as HfO_2-based dielectric is used.

3. The work function of MoN_x increases with the increase of nitrogen content and tends to saturate at the valence band of Si. No Fermi-pinning effect is observed on HfO_2 film.

4. The work function and thermal stability of MoN_x show good thermal stability on both SiO_2 and HfO_2 films up to 800°C at least.

According to these results, MoN_x is a promising gate material for pMOSFETs. The high resistivity of the metal nitride could be solved by stack structure which consists of a low-resistivity top layer and a metal nitride bottom layer. The top layer is used to reduce the sheet resistance and the bottom layer is used to control the threshold voltage. In this scheme, Mo/MoN stack might be a good choice.

Acknowledgment

This work was supported by the National Science Council, Republic of China, under contract no. NSC-92-2215-E-009-001.

National Chiao Tung University assisted in meeting the publication costs of this article.

References

1. International Technology Roadmap for Semiconductors (ITRS), 2003 ed., Semiconductor Industry Association (SIA), http://public.itrs.net
2. R. Lin, Q. Lu, P. Ranade, T.-J. King, and C. Hu, *IEEE Electron Device Lett.*, **23**, 49 (2002).
3. B. Cheng, B. Matti, S. Samayedam, J. Grant, B. Taylor, P. Tobin, and J. Mogab, in *Proceedings of the IEEE International SOI Conference*, p. 91 (2001).
4. J. Pan, C. Woo, M.-V. Ngo, P. Besser, J. Pellerin, Q. Xiang, and M.-R. Lin, *IEEE Electron Device Lett.*, **24**, 547 (2003).
5. J. Pan, C. Woo, M.-V. Ngo, C.-Y. Yang, P. Besser, P. King, J. Bernard, E. Adem, B. Tracy, J. Pellerin, Q. Xiang, and M.-R. Lin, *IEEE Trans. Electron Devices*, **ED-50**, 2456 (2003).
6. C. Ren, H. Y. Yu, J. F. Kang, X. P. Wang, H. H. H. Ma, Y.-C. Yeo, D. S. H. Chan, M. F. Li, and D.-L. Kwong, *IEEE Electron Device Lett.*, **25**, 580 (2004).
7. A. Chatterjee, R. A. Chapman, G. Dixit, J. Kuehne, S. Hattangady, H. Yang, G. A. Brown, R. Aggarwal, U. Erdogan, Q. He, M. Hanratty, D. Rogers, S. Murtaza, S. J. Fang, R. Kraft, A. L. P. Rotondaro, J. C. Hu, M. Terry, W. Lee, C. Fernando, A. Konecni, G. Wells, D. Frystak, C. Bowen, M. Rodder, and I.-C. Chen, *Tech. Dig. - Int. Electron Devices Meet.*, **1997**, 821.
8. C. S. Park, B. J. Cho, and D.-L. Kwong, *IEEE Electron Device Lett.*, **24**, 298 (2003).
9. H.-Y. Yu, M.-F. Li Sr., and D.-L. Kwong, *IEEE Trans. Electron Devices*, **ED-51**, 609 (2004).
10. A. Vandooren, S. Egley, M. Zavala, T. Stephens, L. Mathew, M. Rossow, A. Thean, A. Barr, Z. Shi, T. White, D. Pham, J. Conner, L. Prabhu, D. Triyoso, J. Schaeffer, D. Roan, B.-Y. Nguyen, M. Orlowski, and J. Mogab, *IEEE Trans. Nanotechnol.*, **2**, 324 (2003).
11. Q. Lu, Y. C. Yeo, P. Ranade, H. Takeuchi, C. Hu, S. C. Song, H. F. Luan, and D.-L. Kwong, in *Proceedings of the IEEE Symposium on VLSI Technology*, p. 72 (2000).
12. Y.-C. Yeo, Q. Lu, P. Ranade, H. Takeuchi, K. J. Yang, I. Polishchuk, T.-J. King, C. Hu, S. C. Song, H. F. Luan, and D.-L. Kwong, *IEEE Electron Device Lett.*, **22**, 227 (2001).
13. P. Ranade, Y. C. Yeo, Q. Lu, H. Takeuchi, T.-J. King, and C. Hu, *Mater. Res. Soc. Symp. Proc.*, **2000**, 611.
14. Q. Lu, R. Lin, P. Ranade, Y. C. Yeo, X. Meng, H. Takeuchi, T. J. King, C. Hu, H. Luan, S. Lee, W. Bai, C.-H. Lee, D.-L. Kwong, X. Gau, X. Wang, and T.-P. Ma, *Tech. Dig. - Int. Electron Devices Meet.*, **2000**, 641.
15. M. J. Kim and D. M. Brown, *IEEE Trans. Electron Devices*, **ED-30**, 598 (1983).
16. S.-I. Ohfuji, C. Hashimoto, T. Amazawa, and J. Murota, *J. Electrochem. Soc.*, **131**, 446 (1984).
17. H. B. Michaelson, *J. Appl. Phys.*, **48**, 4729 (1977).
18. P. Ranade, Y.-K. Choi, D. Ha, A. Agarwal, M. Ameen, and T.-J. King, *Tech. Dig. - Int. Electron Devices Meet.*, **2002**, 363.
19. Y.-K. Choi, L. Chang, P. Ranade, J.-S. Lee, D. Ha, S. Balasubramanian, A. Agarwal, M. Ameen, T.-J. King, and J. Bokor, *Tech. Dig. - Int. Electron Devices Meet.*, **2002**, 259.
20. Q. Lu, R. Lin, P. Ranade, T.-J. King, and C. Hu, in *Proceedings of the IEEE Symposium on VLSI Technology*, p. 45 (2001).
21. P. Ranade, H. Takeuchi, T.-J. King, and C. Hu, *Electrochem. Solid-State Lett.*, **4**, G85 (2001).
22. Y.-C. Yeo, P. Ranade, T.-J. King, and C. Hu, *IEEE Electron Device Lett.*, **23**, 342 (2002).
23. Y.-C. Yeo, T.-J. King, and C. Hu, *J. Appl. Phys.*, **92**, 7266 (2002).
24. H. Y. Yu, C. Ren, Y.-C. Yeo, J. F. Kang, X. P. Wang, H. H. H. Ma, M.-F. Li, D. S. H. Chan, and D.-L. Kwong, *IEEE Electron Device Lett.*, **25**, 337 (2004).
25. C. Ren, H. Y. Yu, J. F. Kang, Y. T. Hou, M.-F. Li, W. D. Wang, D. S. H. Chan, and D.-L. Kwong, *IEEE Electron Device Lett.*, **25**, 123 (2004).
26. C. C. Hobbs, L. R. C. Fonseca, A. Knizhnik, V. Dhandapani, S. B. Samavedam, W. J. Taylor, J. M. Grant, L. G. Dip, D. Roan, M. L. Lovejoy, R. S. Rai, E. A. Hebert, H.-H. Tseng, S. G. H. Anderson, B. E. White, and P. J. Tobin, *IEEE Trans. Electron Devices*, **ED-51**, 971 (2004).
27. Y. Taur and T. H. Ning, *Fundamentals of Modern VLSI Device*, p. 75, Cambridge University Press, Cambridge, U.K. (1988).
28. R. Jha, J. Gurganos, Y. H. Kim, R. Choi, and J. Lee, *IEEE Electron Device Lett.*, **25**, 420 (2004).
29. H. Jehn and P. Ettmayer, *J. Less-Common Met.*, **58**, 85 (1978).
30. K. Nakajima, Y. Akaska, and M. Kaneko, in *Proceedings of the IEEE Symposium on VLSI Technology*, p. 95 (1999).
31. C. F. Huang and B. Y. Tsui, in *Proceedings of the International Conference on Solid State Devices and Materials (SSDM)*, p. 506 (2005).
32. H. Y. Yu, C. Ren, Y. Yeo, J. F. Kang, X. P. Wang, H. H. H. Ma, M. Li, D. S. H. Chan, and D. Kwong, *IEEE Electron Device Lett.*, **25**, 337 (2004).